Journal of Materials Chemistry

Cite this: J. Mater. Chem., 2012, 22, 5374

www.rsc.org/materials

PAPER

New full-color-emitting phosphor, Eu^{2+}-doped $Na_{2-x}Al_{2-x}Si_xO_4$ ($0 \leq x \leq 1$), obtained using phase transitions for solid-state white lighting†

Ji Yeon Han,[a] Won Bin Im,[b] Donghyuk Kim,[a] Sang Hoon Cheong,[a] Ga-yeon Lee[a] and Duk Young Jeon*[a]

Received 28th October 2011, Accepted 27th December 2011
DOI: 10.1039/c2jm15501j

A new color-tunable Eu^{2+}-doped sodium aluminium silicate, $Na_{2-x-y}Al_{2-x}Si_xO_4{:}yEu^{2+}$ ($0 \leq x \leq 1$), phosphor system was investigated as a novel candidate for phosphor-converted white light-emitting diode (LED) applications and successfully synthesized by wet chemical methods based on the hydrolysis of tetraethyl orthosilicate (TEOS). Different crystal structures and emission spectra were obtained by varying the ratio of Al to Si in the phosphor $Na_{2-x}Al_{2-x}Si_xO_4$ with x value ranging from 0.25 to 0.55. The $Na_{2-x-y}Al_{2-x}Si_xO_4{:}yEu^{2+}$ phosphor system emitted a maximum intensity at 470–600 nm when using a 395 nm excitation wavelength, and the emission was strongly affected by the crystal structures determined by the x value. Substitution of Eu^{2+} affected the center wavelength and emission intensity due to changes in the crystal-field effect, which was strongly dependent on the crystal structure. The LED device exhibited an excellent color-rendering index R_a of 93 at a correlated color temperature of 4258 K with CIE color coordinates of (0.3629, 0.3427) under a 20 mA forward-bias current. Based on these results, we are currently evaluating the potential application of $Na_{2-x-y}Al_{2-x}Si_xO_4{:}yEu^{2+}$ as a white-emitting UV-convertible phosphor.

1. Introduction

White light-emitting diodes (LEDs) have been used more frequently as illumination light sources over the past several years because white LEDs can provide significant power savings, long lifetime (>100 000 h), high luminous efficiency, and environmental friendliness.[1,2] An LED-based light is fabricated using the combination of a blue-emitting LED chip with a yellow-emitting $Y_3Al_5O_{12}{:}Ce^{3+}$ (YAG:Ce^{3+}) phosphor; this combination is widely used due to an unsurpassed efficiency (>30 lm W^{-1}).[3,4] Although a blue-emitting LED chip with a yellow-emitting YAG:Ce^{3+} phosphor has a high efficiency, it has a poor color-rendering index because YAG:Ce^{3+} phosphors have a relatively weak emission in the red spectral region, and it is difficult to obtain good color rendering as measured by the index (R_a).[5,6] Furthermore, phosphors, with the exception of YAG:Ce^{3+}, have a weak or no absorption band in the range of 440–460 nm. Recently, the use of near-ultraviolet LEDs (near-UV LEDs), a new class of white LEDs, combined with multi-component phosphors has been attempted to overcome these drawbacks, and there have been extensive efforts to develop new phosphors for near-UV-pumped LED applications.[7–10] Near-UV-pumped LEDs with multi-component phosphors can offer superior color uniformity, a high color-rendering index ($R_a > 90$), and excellent light quality. In this article, we report a new Eu^{2+}-doped phosphor, $Na_{2-x}Al_{2-x}Si_xO_4{:}Eu^{2+}$ ($0 \leq x \leq 1$), that is potentially applicable to white LEDs. The crystal structure of $Na_{2-x}Al_{2-x}Si_xO_4$ is highly similar to that of the cristobalite-like structure of silicon dioxide, which is an important industrial material because of its excellent mechanical properties, such as a high chemical and thermal stability. The persistence of cristobalite outside of its thermodynamic stability range occurs because the transition from the α-phase to the β-phase requires breaking up and reforming the silica framework. In addition, the tetrahedral units of the framework structures are usually very stiff but are rather loosely joined at the shared corner atoms with a constant bond-bending force at the corners. A rich variety of structures results from the many different ways in which tetrahedra can be linked to form corner-sharing arrays. The structure of $Na_{2-x}Al_{2-x}Si_xO_4$ is similar to that of β-cristobalite, which is described as a "stuffed" cristobalite, and the stuffed cristobalite can be derived from β-cristobalite by partial cross-substitution of Si^{4+} with Al^{3+}; β-cristobalite is subsequently stabilized by trapping Na^+ cations in the interstices of the (Si,Al)-O_4 network. The charge imbalance caused by the substitution of Al^{3+} for Si^{4+} induces crystal distortion, and a crystal structure transition occurs. The synthetic composition $Na_{2-x}Al_{2-x}Si_xO_4$ is well known as a sodium aluminate–carnegieite system with five

[a]Department of Materials Science and Engineering, Korea Advanced Institute of Science and Technology, 291 Daehak-ro, Yuseong-gu, Daejeon, 305-701, Republic of Korea. E-mail: dyjeon@kaist.ac.kr
[b]School of Materials Science and Engineering, Chonnam National University, 300 Yongbong-Dong, Buk-Gu, Gwangju, 500-757, Republic of Korea

† Electronic supplementary information (ESI) available. See DOI: 10.1039/c2jm15501j

different structure types based on distortions of the ideal β-cristobalite structure type.[11,12] The distorted β-cristobalite type of structures has a continuous channel parallel to the *c* direction and two large interstitial sites at 1/2,1/2,1/2 and 3/4,3/4,3/4 in the Na^+ channel.[11] In this study, these interstitial Na^+ sites have been used as activator sites for Eu^{2+} cations to provide luminescence. Eu^{2+}-doped silicate generally shows superior absorption in the spectral region of 250–400 nm, and because the 4*f*–5*d* transition of the Eu^{2+} ion is sensitive to the crystal field and covalency, the Eu^{2+}-doped silicate has strong absorption in the UV-to-visible spectral region and exhibits broad emission bands from blue to red.[13,14] $Na_{2-x}Al_{2-x}Si_xO_4$ is expected to be a good candidate as a host material due to its strong absorption in the UV/blue light spectral region, its long wavelength emissions, and material design flexibility based on the simplicity of changing the (Si,Al)-O_4 network.

In this study, the structure and optical properties of a new color-tunable phosphor system, $Na_{2-x}Al_{2-x}Si_xO_4:Eu^{2+}$, were investigated. To the best of our knowledge, there has been no reported study on the $Na_{2-x}Al_{2-x}Si_xO_4$ composition system as a phosphor host. For the first time, a wet chemical synthesis method was applied for the synthesis of a $Na_{2-x}Al_{2-x}Si_xO_4:Eu^{2+}$ phosphor based on the hydrolysis of tetraethyl orthosilicate (TEOS). In general, solid state methods are widely used for the synthesis of phosphors; however, it is difficult to control the stoichiometry of complex compositions, such as $Na_{2-x}Al_{2-x}Si_xO_4:Eu^{2+}$, using this method. In this study, the $Na_{2-x}Al_{2-x}Si_xO_4:Eu^{2+}$ phosphor was synthesized successfully. In addition, the emission color of synthesized $Na_{2-x}Al_{2-x}Si_xO_4:Eu^{2+}$ ($0 \le x \le 1$) phosphors can be easily tailored from blue to orange *via* tuning of the *x* value. This paper also reports the dependency of the emission properties of the $Na_{2-x}Al_{2-x}Si_xO_4:Eu^{2+}$ ($0 \le x \le 1$) phosphors upon the Eu concentration. Finally, we succeeded in fabricating white-emitting UV LEDs and thoroughly examined their optical properties.

2. Experimental

2.1 Sample preparation

Powder samples of $Na_{2-x}Al_{2-x}Si_xO_4:Eu^{2+}$ ($0 \le x \le 1$) were prepared by the solution method using proper amounts of aluminium nitrate nonahydrate ($Al(NO_3)_3 \cdot 9H_2O \ge 98\%$, Aldrich), sodium nitrate ($NaNO_3 \ge 99.99\%$, Aldrich), tetraethyl orthosilicate (TEOS; $Si(OC_2H_5)_4$, 99.999%; Aldrich), and europium(III) chloride hexahydrate ($EuCl_3 \cdot 6H_2O$, 99.99%; Aldrich) as starting materials. All materials were dissolved in water (solution A) with the exception of TEOS, which was mixed with ethanol (solution B). After solutions A and B were prepared, they were thoroughly mixed together. Subsequently, a transparent mixture solution was obtained that had a pH <2. The mixtures were dehydrated in an oven at 120 °C until the solvent dried completely. The dried powders were then annealed at 1300 °C in a reducing atmosphere of H_2/N_2 (5%/95%) for 3 h. During a preliminary study, we observed that annealing at temperatures >1300 °C led to a significant loss of Na. The solution method was based on TEOS hydrolysis. TEOS is generally used as an Si source according to the following reaction equation:[15]

$$Si(OC_2H_5)_4 + 4H_2O \rightarrow Si(OH)_4 + 4C_2H_5OH$$
in ethanol at pH <2

2.2 Characterization

Room-temperature photoluminescence (PL) spectra were recorded using a Hitachi F-7000 fluorescence spectrophotometer PL system equipped with a xenon lamp (500 W) as an excitation source scanning the wavelength of 400–800 nm. X-Ray diffraction (XRD) data were obtained over a range of $10° \le 2\theta \le 120°$ at 0.026° steps using a Cu-Kα radiation source (Philips X'Pert). Crystal structure refinement employed the Rietveld method as implemented in the General Structure Analysis System (GSAS) software suite.[16] For time-resolved PL measurements, frequency-tripled Ti:sapphire laser pulses (~100 fs; Mira 900) were used to excite the phosphor at a wavelength of 390 nm, and a commercial time-correlated single-photon counting system was used for detection.

2.3 Fabrication of white LEDs

In the white LED fabrication, near-UV LED chips (λ_{max} = 395 nm) were combined with $Na_{2-x}Al_{2-x}Si_xO_4:Eu^{2+}$ phosphors, a blue-emitting $BaMgAl_{10}O_{17}:Eu^{2+}$ phosphor, and green-emitting $Ba_2SiO_4:Eu^{2+}$ phosphors. Optical properties, such as the luminescence spectra, color-rendering index (R_a), and Commission International de l'Eclairage (CIE) color coordinates of the white LEDs, were characterized using an Xe lamp (500 W) with a DARSA PRO 5100 PL system (PSI Scientific Co. Ltd., Korea) and evaluated under varied forward biases of constant currents in which the light output was collected and measured using an integrating sphere.

3. Results and discussion

3.1 XRD refinement and crystal structure

Fig. 1 shows the composition phase diagram of the Eu^{2+}-doped sodium aluminate–carnegieite $Na_{2-x}Al_{2-x}Si_xO_4:Eu^{2+}$ ($0 \le x \le 1$) system. An orthorhombic-type structure was obtained from $Na_{2-x}Al_{2-x}Si_xO_4:Eu^{2+}$ at $x = 0.25$. At $x = 0.35$, tetragonal phase was observed, whereas a cubic β-cristobalite-type structure was observed at $x = 0.55$.[11,12,17] In the $Na_{2-x}Al_{2-x}Si_xO_4:Eu^{2+}$ phosphor system, it is assumed that Eu^{2+} ($r = 0.117$ nm when coordinate number (CN) = 6 and $r = 0.100$ nm when CN = 7) ions occupied the Na^+ ($r = 0.102$ when CN = 6) sites because both the Al^{3+} ($r = 0.039$ nm) and the Si^{4+} ($r = 0.026$ nm) sites are too small to take the Eu^{2+} ions.[18] To control the *x* values in the $Na_{2-x}Al_{2-x}Si_xO_4:Eu^{2+}$ system, the ratio of Al or Na to the Si content was controlled. Table 1 gives the results of the preparation

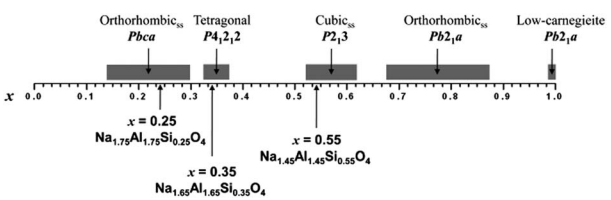

Fig. 1 Composition phase diagram of $Na_{2-x}Al_{2-x}Si_xO_4$ ($0 \le x \le 1$).

Table 1 Products formed with different concentrations of excess Na and Al ions in the reaction mixture

	Na : Al : Si			
Serial no.	Reaction mixture	Product	Crystal structure	JCPDS #
1	0.8 : 0.8 : 1	1 : 1 : 1	Low-carnegieite	78-1858
2	1.4 : 1.4 : 1	1 : 1 : 1 + 1.15 : 1.15 : 0.85	Low-carnegieite + orthorhombic	78-1858 + 49-0007
3	2 : 2 : 1	1.45 : 1.45 : 0.55	Cubic	49-0002
4	2.6 : 2.6 : 1	1.45 : 1.45 : 0.55 + 1.55 : 1.55 : 0.45	Cubic + orthorhombic	49-0002 + 49-0006
5	3.2 : 3.2 : 1	1.65 : 1.65 : 0.35	Tetragonal	49-0005
6	3.8 : 3.8 : 1			
7	4.4 : 4.4 : 1	1.75 : 1.75 : 0.25	Orthorhombic	49-0004
8	5 : 5 : 1			
9	5.6 : 5.6 : 1			

with different mole ratios of $NaNO_3$ or $Al(NO_3)_3$: TEOS (as a Si source). The initial phase was $Na_{1.45}Al_{1.45}Si_{0.55}O_4$ with a 2 : 1 ratio of $NaNO_3$ or $Al(NO_3)_3$ to TEOS.[12] When the ratio of the $NaNO_3$ or $Al(NO_3)_3$ to TEOS was varied from 0.8 : 1 to 5.6 : 1, the $Na_{2-x}Al_{2-x}Si_xO_4$:Eu^{2+} phase was regulated.

Upon the addition of Al, the Na content was more than double the Si content, the substitution of Si^{4+} sites with Al^{3+} ions increased, and additional Na^+ was needed to compensate for the charge. This finding demonstrated that the ratio between $NaNO_3$ and $Al(NO_3)_3$ had the same mole value. As Al^{3+} ions substituted into the Si^{4+} sites, a structure distortion occurred; as a result, an x value-dependent phase change was observed. At lower Al contents, the $Na_{1.45}Al_{1.45}Si_{0.55}O_4$ ($x = 0.55$), $NaAlSiO_4$ ($x = 1$), and $Na_{1.15}Al_{1.15}Si_{0.85}O_4$ ($x = 0.85$) structures were dominant; however, as the Al content increased, the $Na_{1.45}Al_{1.45}Si_{0.55}O_4$ ($x = 0.55$) system and the tetragonal $Na_{1.65}Al_{1.65}Si_{0.35}O_4$ ($x = 0.35$) and orthorhombic $Na_{1.75}Al_{1.75}Si_{0.25}O_4$ ($x = 0.25$) mixture phases were observed. Finally, a phase of orthorhombic $Na_{1.75}Al_{1.75}Si_{0.25}O_4$ ($x = 0.25$) was obtained when the Al content was 4.4-fold higher than the Si content. We demonstrated that crystal distortions of the $Na_{2-x}Al_{2-x}Si_xO_4$:Eu^{2+} phosphor systems are generated by the different ratios of Al to Si.[17] The crystal structure of the $Na_{2-x}Al_{2-x}Si_xO_4$:Eu^{2+} phosphor system was strongly dependent on the x value, which was controlled by the Al and Na contents in the $Na_{2-x}Al_{2-x}Si_xO_4$:Eu^{2+} system and induced the crystal distortion. Increasing Al and Na contents resulted in a decreased x value, which led to a change in the crystal structure from orthorhombic ($x = 0.85$) to cubic ($x = 0.55$) to orthorhombic ($x = 0.45$) to tetragonal ($x = 0.35$) and finally to orthorhombic ($x = 0.25$). In this study, the three phases—cubic, tetragonal, and orthorhombic—were represented by the $Na_{2-x}Al_{2-x}Si_xO_4$:Eu^{2+} phosphor systems.

To obtain the crystal properties of the $Na_{2-x}Al_{2-x}Si_xO_4$ with varied x values, a Rietveld refinement using X-ray powder diffraction was performed. Fig. 2 shows the Rietveld refinement of the XRD profiles of a $Na_{2-x}Al_{2-x}Si_xO_4$ sample series ($x = 0.25$, 0.35, and 0.55). Based on the Rietveld refinement results, negligible amounts of impurity phases were identified in the samples. Initial structural models to approximate the actual $Na_{2-x}Al_{2-x}Si_xO_4$ structure were constructed using previously reported crystallographic data.[18] The final weighted R factors (R_{wp}) of the samples were successfully converged at a satisfactory level, and the refined structural parameters of $Na_{2-x}Al_{2-x}Si_xO_4$ are listed in Table 2.

Fig. 3 displays the unit cell of the $Na_{2-x}Al_{2-x}Si_xO_4$:Eu^{2+} representation with various x values. The parent structure of all of the sodium aluminate–carnegieite samples is a partially stuffed $C9$ structure with an ideal cubic lattice parameter, in which some proportion of the 12-coordinate interstitial sites is filled with Na^+ to balance the negative charge created by the substitution of Si

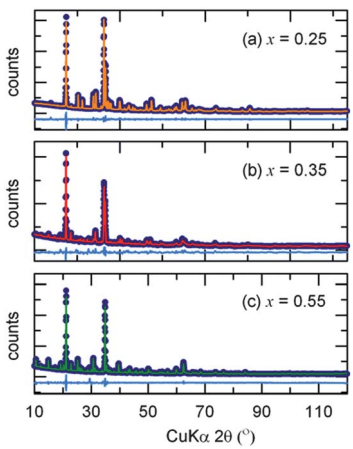

Fig. 2 Rietveld refinement results of the powder X-ray diffraction profile of $Na_{2-x}Al_{2-x}Si_xO_4$ phosphors with varying Si concentration x values.

Table 2 Rietveld refinement and crystal property data of $Na_{2-x}Al_{2-x}Si_xO_4$ phosphors[a]

Formula	$x = 0.25$	$x = 0.35$	$x = 0.55$
Radiation type	CuKα	CuKα	CuKα
2θ range (degree)	10–120	10–120	10–120
T/K	295	295	295
Symmetry	Orthorhombic	Tetragonal	Cubic
Space group	*Pbca*	$P4_12_12$	$P2_13$
a/Å	10.451(2)	10.385(1)	14.577(5)
b/Å	14.291(6)	—	—
c/Å	5.2186(3)	7.178(5)	—
Z	8	8	32
R_p	4.95%	4.79%	5.52%
R_{wp}	6.85%	7.10%	3.85%
χ^2	9.518	11.36	7.16

[a] The numbers in parentheses are the estimated standard deviations of the last significant figure.

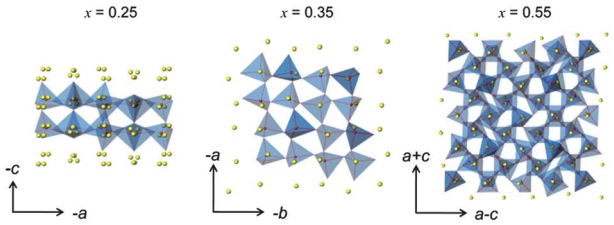

Fig. 3 Unit cell representation of $Na_{2-x}Al_{2-x}Si_xO_4:Eu^{2+}$ phosphors along the [010] axis according to x values 0.25, 0.35, and 0.55. The red, yellow, and blue spheres represent Al or Si, Na, and O atoms, respectively.

with Al in the tetrahedral framework.[12] The O-atom sites are always fully occupied, whereas the average occupancies of the framework metal and Na^+ sites are dependent upon the $Na_{2-x}Al_{2-x}Si_xO_4:Eu^{2+}$ composition. The ideal *C*9-type parent structures for the $x = 0.25$, 0.35, and 0.55 phases have cubic unit-cell parameters of 8.038, 8.008, and 7.964 Å, respectively.[17] The stuffed *C*9 structure shows remarkably diverse chemistry attributable to the intrinsic flexibility of the Al–O–Si linkages.

3.2 Photoluminescence properties

Variations in the excitation (PLE) and emission (PL) spectra of the three $Na_{2-x}Al_{2-x}Si_xO_4:Eu^{2+}$ phosphor systems depending on the x value are shown in Fig. 4a and b, respectively. In the PLE spectra, the excitation peaks of the $Na_{2-x}Al_{2-x}Si_xO_4:Eu^{2+}$ phosphor systems were recorded at 250–500 nm. The excitation band corresponds to the transition from the $4f^7$ ground state to the $4f^65d$ excited state of an Eu^{2+} ion.[19] Fig. 4b shows the dominant emission wavelengths of $Na_{2-x}Al_{2-x}Si_xO_4:Eu^{2+}$ at various x values, which demonstrates that full-color emission was realized *via* changing of the x value in the three phosphor systems. The asymmetric emission spectra show that the Eu^{2+} ions have more than one emission center in the lattice. Consequently, it was deconvoluted into Gaussian components indicating different symmetry sites of the Eu^{2+} ion.

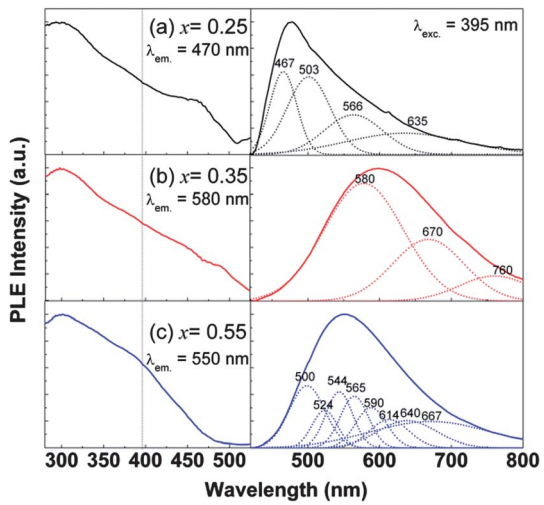

Fig. 4 Normalized PL spectra: (a) excitation and (b) emission of $Na_{2-x}Al_{2-x}Si_xO_4:Eu^{2+}$ phosphor systems as a function of the x value.

By Gaussian deconvolution, the emission spectra of the $Na_{2-x}Al_{2-x}Si_xO_4:Eu^{2+}$ at various x values can be decomposed into 4, 3, and 8 Gaussian profiles with peaks centered at 467 nm (21 413 cm^{-1}), 503 nm (19 880 cm^{-1}), 566 nm (17 667 cm^{-1}), and 635 nm (15 748 cm^{-1}) (Fig. 4a, black dotted lines) and 580 nm (17 241 cm^{-1}), 670 nm (14 925 cm^{-1}), and 760 nm (13 157 cm^{-1}) (Fig. 4b, red dotted lines) and 500 nm (20 000 cm^{-1}), 524 nm (19 083 cm^{-1}), 544 nm (18 382 cm^{-1}), 565 nm (17 699 cm^{-1}), 590 nm (16 949 cm^{-1}), 614 nm (16 286 cm^{-1}), 640 nm (15 625 cm^{-1}), and 667 nm (14 992 cm^{-1}) (Fig. 4c, blue dotted lines), respectively. These peaks can be ascribed to different emission sites, which could be identified as the different coordination environments (Table S1†) of the Na^+ ions being occupied by Eu^{2+} ions (ESI†). Variations in the excitation and emission spectra were attributed to changes in the environment surrounding the Eu^{2+} ions originated from different symmetry sites. The $4f^7 \rightarrow 4f^65d$ transition of Eu^{2+} is strongly dependent on the host lattice because the outermost 5*d* orbit is highly sensitive to its crystal-field surroundings.[20,21] Upon excitation at a wavelength of 395 nm, the internal quantum efficiencies of phosphors were found to be 2%, 6.5%, and 10.2% for $x = 0.25$, 0.35, and 0.55, respectively, as shown in Table 3. The various emission bands at 470–600 nm, which had wider full widths at half maximum (FWHM) than at 120 nm, were observed at different x values of 0.25–0.55. This finding implies that the incorporation of $Na_{2-x}Al_{2-x}Si_xO_4:Eu^{2+}$ into white LEDs may provide an improved color-rendering index.

Fig. 5 shows the emission spectra and dominant emission wavelength as a function of Eu^{2+} concentration in three structural systems with varied x values. In general, the phosphor at $x = 0.25$ shows a blue to yellow emission consisting of more than one emission band. The 470 nm blue emission is dominant at lower Eu^{2+} concentration, although 550 nm yellow emission appears as the Eu^{2+} concentration increases; at the same time, the 470 nm emission decreases, and the 550 nm emission increases. The asymmetric emission can be explained by the change of relative intensity among the four Gaussian components as shown in Table S2 and Fig S1 (ESI†). The phosphor at $x = 0.35$ has a yellow to orange emission of 555–600 nm. The phosphor at $x = 0.35$ shows increased PL intensity with increasing Eu^{2+} concentration. The phosphor at $x = 0.55$ shows yellow emission of 550–555 nm. The emission bands of all phosphors with various x values have systematic red-shifts as the Eu^{2+} concentration increases due to reduced lattice rigidity and crystal field change-induced splitting of Eu^{2+} 5d electrons. The dependence of the peak position on the Eu^{2+} ion concentration is shown in Fig. 5d. Unlike the increased PL intensity of the two phosphors with $x = 0.35$ and 0.55, the PL intensity decreased with increasing Eu^{2+} concentrations in the $x = 0.25$ systems. The difference in

Table 3 Spectral parameters for the $Na_{2-x}Al_{2-x}Si_xO_4:Eu^{2+}$ phosphor systems, quantum efficiency (QY), peak position of PL (P_{em}), and emission width ($FWHM_{em}$)

x Value	QY (%)	P_{em}/nm	$FWHM_{em}$/nm
0.55	10.2	550	155
0.35	6.5	600	180
0.25	2	470	175

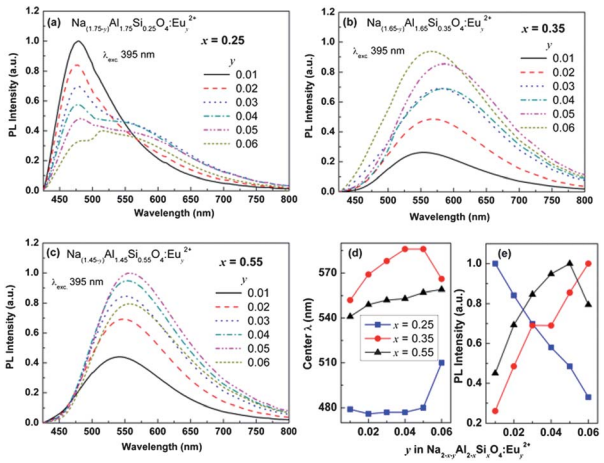

Fig. 5 Emission spectra of (a) $x = 0.25$, (b) $x = 0.35$, (c) $x = 0.55$, and (d) center wavelength of PL as well as (e) maximum PL intensity as a function of the Eu^{2+} concentration.

emission behavior of these three phosphor systems with different x values is due to the different local structures around the Eu^{2+} ions. When Eu^{2+} substituted for singly charged Na^+, the charge-compensating positive ion vacancy is necessary and it is expected to be located at one of the nearest Na^+ sites around the Eu^{2+} ion. The position of vacancy strongly depends on the nearest-neighbor Na^+ site and induces three different site symmetries, tetragonal C_{4v}, trigonal C_{3v}, and orthorhombic C_{2v} for the Eu^{2+} ion. As the crystal structure of the phosphor system changes, the local surroundings of the Eu^{2+}-substituted sites are significantly changed due to bond-length changes between the activator cation and the ligand anion. The different crystal structures cause changes to the local surroundings of the Eu^{2+}-substituted sites, namely a different crystal field. Crystal field splitting (D_q) is expressed as follows:[22]

$$D_q = \frac{1}{6} Ze^2 \frac{r^4}{R^5} \quad (1)$$

where D_q is a measure of the energy level separation, Z is the valence charge of the anion ligand, e is the electron charge, r is the radius of the d-wave function, and R is the bonding length between the activator cation and the ligand anion. When Na^+ is substituted by the larger Eu^{2+} ion, the distance between Eu^{2+} and O^{2-} becomes shorter, and the magnitude of the crystal field increases; as a result, the $5d$ band of Eu^{2+} is decreased, and the emission wavelength is red-shifted with increasing Eu^{2+} concentrations in all of the $Na_{2-x}Al_{2-x}Si_xO_4$:Eu^{2+} phosphor systems regardless of the x value. As shown in Fig. 5e, the optimum Eu^{2+} concentrations of the $x = 0.25$, 0.35, and 0.55 systems were found to be 0.01, 0.05, and 0.05, respectively, and their optimized emission intensities were observed at those points. A continuously increased emission intensity (up to 0.05 mol) was seen for the $x = 0.35$ system due to phase transition.

The decrease in emission intensity beyond a critical concentration of Eu^{2+} can be explained by concentration quenching. This is mainly caused by the energy transfer among Eu^{2+} ions in the $Na_{2-x}Al_{2-x}Si_xO_4$ lattice, which results in non-radiative energy, and the non-radiative transition increases with increasing Eu^{2+} content.[23] A plausible reason for the different concentration-quenching behaviors may be the symmetry-related energy transfer behavior. The concentration-quenching behaviors also suggest that the Eu^{2+} ions in the $x = 0.25$ phosphor system are located in a heavily distorted cation environment relative to Eu^{2+} in the $x = 0.55$ phosphor system. The characteristic of concentration quenching of $Na_{2-x}Al_{2-x}Si_xO_4$:0.05Eu^{2+} phosphors can be confirmed through the observed dependence of the fluorescence decay curves on the x values. A long decay time is characteristic of most symmetrical surroundings, whereas a shorter decay time can be observed when site distortion occurs.[24,25] It might be presumed that the distorted crystal has a higher number density of defect impurities that act as quenching sites. With increasing quenching sites, nonradiative transition is dominant and shows decreased radiative decay time according to the relationship $1/\tau_{measured} = 1/\tau_{radiative} + 1/\tau_{nonradiative}$.

The decay processes for $Na_{2-x}Al_{2-x}Si_xO_4$:Eu^{2+} phosphors were also investigated and are shown in Fig. 6. The corresponding luminescent decay times monitored at 390 nm excitation can be fitted well with a second-order exponential decay curve using the following equation:[26,27]

$$I = A_1 \exp(-t/\tau_1) + A_2 \exp(-t/\tau_2) \quad (2)$$

where I is the luminescence intensity, A_1 and A_2 are constants, t is the time, and τ_1 and τ_2 are the respective short and long lifetimes for the exponential components. Using these parameters, the average decay time (τ^*) can be determined using the following formula:[28]

$$\tau^* = (A_1\tau_1^2 + A_2\tau_2^2)/(A_1\tau_1 + A_2\tau_2) \quad (3)$$

The average decay times of the $x = 0.25$ (orthorhombic) and $x = 0.35$ (tetragonal) systems are 0.17 and 0.20 μs, respectively, whereas that of the $x = 0.55$ (cubic) system is 0.57 μs. The lattice distortion increased with decreasing x, and the progressive substitution of Al with Si was seen in the tetrahedral framework sites.[17] When the x value decreased, the $Na_{2-x}Al_{2-x}Si_xO_4$:Eu^{2+}

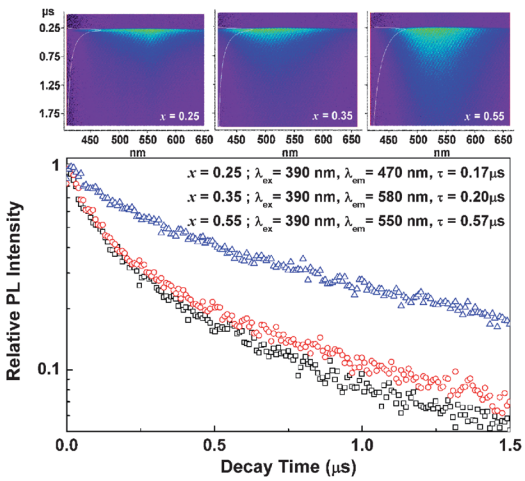

Fig. 6 The decay curves for the emission band of Eu^{2+} as a function of the x value at 470, 550, and 580 nm.

phosphor systems showed further lattice distortion, which led to many Eu^{2+} ions occupying lower-symmetry sites, thereby accelerating the decay curve speed and reducing the decay time.

The substituting Eu^{2+} ion is accompanied by a charge-compensating cation vacancy in one of the adjacent Na^{+} ion sites in the $Na_{2-x}Al_{2-x}Si_xO_4:Eu^{2+}$ phosphor system. The charge-compensating vacancy is required to be located close to the impurity to form a stable Eu^{2+}-vacancy dipole. The site symmetry is C_{2v} for the orthorhombic structure, C_{4v} for the tetragonal structure, and C_{4v} and O_h for the cubic structures. The C_{2v} symmetry of the substituting Eu^{2+} has a stronger coupling with the vacancy than the coupling of Eu^{2+} with the other site symmetries because of the shortened distance between the vacancy and the substituting Eu^{2+}.[29–31] The shortened distance between the vacancy and the Eu^{2+} resulted in shorter decay times in the $x = 0.25$ system. The different site symmetries present in the $Na_{2-x}Al_{2-x}Si_xO_4:Eu^{2+}$ phosphor systems with various x values showed different crystal field splittings. As a result, the shifted central wavelength of the PL emission toward a longer wavelength with various Eu^{2+} concentrations induced full-color emission in the $Na_{2-x}Al_{2-x}Si_xO_4:Eu^{2+}$ (Fig. 7).

3.3 Thermal quenching properties

For the application of white-LEDs, the thermal stability of phosphor is important. Temperature-dependence of relative emission intensities for $Na_{2-x}Al_{2-x}Si_xO_4:Eu^{2+}$ phosphors with various x values under 395 nm excitation is compared in Fig. 8. The relative emission intensities of all phosphor samples decrease with increasing temperature in the range of 25–175 °C. A decay of 48% for $x = 0.25$ (470 nm), 41% for $x = 0.35$ (580 nm), and 21% for $x = 0.55$ (550 nm), respectively, at 150 °C was observed. The inset displays the activation energy (ΔE) of $Na_{2-x}Al_{2-x}Si_xO_4:Eu^{2+}$ phosphors with various x values. The temperature dependence of the emission intensity is described by a modified Arrhenius equation as follows:[32]

$$I_T = \frac{I_0}{1 + A\exp(-\Delta E/kT)} \quad (4)$$

where I_0 is the initial emission intensity, I_T is the intensity at different temperatures, ΔE is the activation energy of thermal quenching, A is a constant for a certain host, and k is the Boltzmann constant (8.617×10^{-5} eV K^{-1}). The ΔE values were

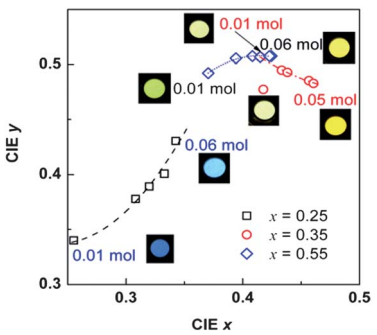

Fig. 7 CIE chromatic coordinates and photoimages of three phosphor systems of $x = 0.25$–0.55 and varying Eu concentrations. The CIE color coordinates of those phosphor systems are depicted as □, ○, and ◇.

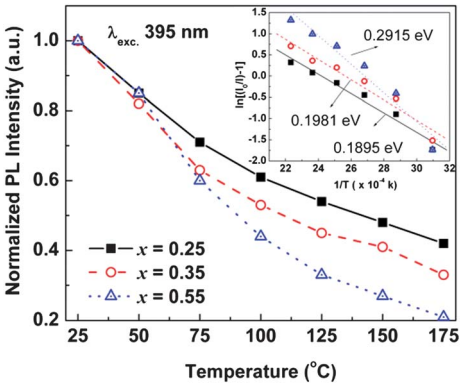

Fig. 8 Temperature-dependent PL intensity of $Na_{2-x}Al_{2-x}Si_xO_4:Eu^{2+}$. The inset shows the activation energy (ΔE) of $Na_{2-x}Al_{2-x}Si_xO_4:Eu^{2+}$ depending on the x value.

obtained to be 0.1895 eV for $x = 0.25$, 0.1981 eV for $x = 0.35$, and 0.2915 eV for $x = 0.55$, respectively.

The $Na_{2-x}Al_{2-x}Si_xO_4:Eu^{2+}$ phosphor with $x = 0.25$ shows higher thermal stability than those of $Na_{2-x}Al_{2-x}Si_xO_4:Eu^{2+}$ phosphors with $x = 0.35$ and 0.55 commodity.

3.4 Electroluminescence (EL) and fabrication of WLEDs

To create LEDs with a high color-rendering index, three types of white LEDs were fabricated using various phosphor combinations together with near-UV-LEDs ($\lambda_{em} = 395$ nm). The white LEDs used a combination of the $Na_{2-x}Al_{2-x}Si_xO_4:Eu^{2+}$ phosphor obtained in this study with blue-emitting $BaMgAl_{10}O_{17}:Eu^{2+}$ and green-emitting $Ba_2SiO_4:Eu^{2+}$ phosphors.

Fig. 9 shows the electroluminescence (EL) of the white LED devices under different forward-bias currents in the range of 20–60 mA. The EL spectra and CIE color coordinates are reported for the following combinations: (a) only $BaMgAl_{10}O_{17}:Eu^{2+}$ mixed in the $x = 0.35$ system; (b) $BaMgAl_{10}O_{17}:Eu^{2+}$ and $Ba_2SiO_4:Eu^{2+}$ mixed with the yellow-emitting $Na_{1.45}Al_{1.45}Si_{0.55}O_4:0.05Eu^{2+}$ phosphor; and (c) the blue-emitting $Na_{1.75}Al_{1.75}Si_{0.25}O_4:0.01Eu^{2+}$ phosphor mixed with orange-emitting $Na_{1.65}Al_{1.65}Si_{0.35}O_4:0.05Eu^{2+}$ phosphor (Fig. 9). As shown in Fig. 9a–c, each phosphor has a broad emission band in the wide wavelength region. Each emission band was clearly located at approximately 450 nm (B), 510 nm (G), 570 nm ($x = 0.55$), 460 nm ($x = 0.25$), and 600 nm ($x = 0.35$). The EL intensity increased continuously as the applied forward bias current increased. This finding indicates that the $Na_{2-x}Al_{2-x}Si_xO_4:Eu^{2+}$ phosphor-based white LED device does not show spectral saturation. The measured optical properties of these white LED devices are also summarized in Table 4. All of the white LED devices from the composite phosphors showed higher R_a values, *i.e.*, (A) $R_a = 88$–90, (B) $R_a = 94$, and (C) $R_a = 91$–93, than those prepared with YAG:Ce^{3+} in a similar manner. In particular, the blue-emitting phosphor with $x = 0.25$ mixed with the orange-emitting phosphor with $x = 0.35$ and the white LEDs (combination C) operated at 20 mA showed a correlated color temperature (CCT) of 4258 K and an excellent R_a of 93. The R_a value is close to that of blue, green, and yellow, *i.e.*, the three components of white LEDs (combination B),

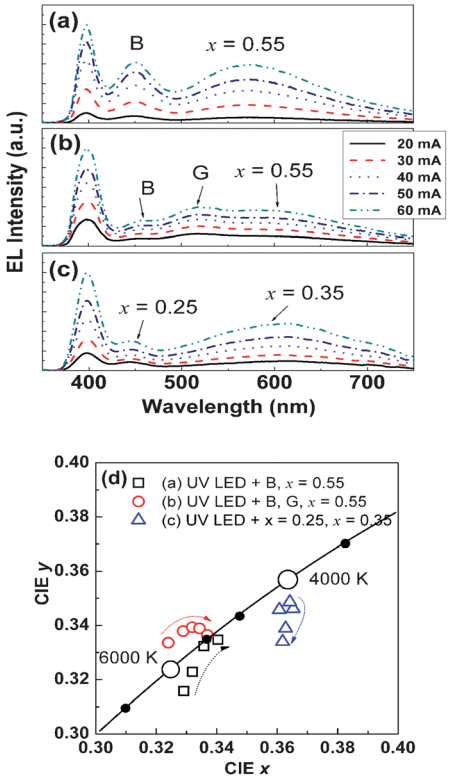

Fig. 9 Luminescence spectra of UV-pumped white LEDs fabricated using various phosphor combinations with UV LEDs (395 nm): (a) $BaMgAl_{10}O_{17}:Eu^{2+}$ (B) + $x = 0.55$ (combination A); (b) $BaMgAl_{10}O_{17}:Eu^{2+}$ (B) + $Ba_2SiO_4:Eu^{2+}$ (G) + $x = 0.55$ (combination B); and (c) $x = 0.25 + x = 0.35$ (combination C).

Table 4 Optical properties of the white LEDs fabricated using various phosphor combinations with UV LEDs ($\lambda_{max} = 395$ nm)

Phosphor	R_a	CIE x	CIE y	Color temperature/K
Combination A	88–90	0.3291–0.3404	0.3158–0.3347	5000–6250
Combination B	94	0.3240–0.3369	0.3336–0.3393	5132–5527
Combination C	91–93	0.3607–0.3653	0.3340–0.3489	4545–4258

although a better color temperature was obtained from blue- and orange-emitting two-component-based white LEDs.

Furthermore, CIE chromaticity coordinates in the ranges of CIE $x = 0.36$ and CIE $y = 0.33$–0.34 were observed. The R_a value is similar to the R_a value of combination B, which combined blue, green, and yellow phosphors. Although the R_a values of the white LEDs combining only $Na_{2-x}Al_{2-x}Si_xO_4:Eu^{2+}$ phosphor systems (combination C) were changed from 93 at 20 mA to 91 at 60 mA, the R_a value is still higher than that of the commercial YAG:Ce^{3+}-based white LED. It is anticipated that the $Na_{2-x}Al_{2-x}Si_xO_4:Eu^{2+}$ phosphor will be considered a promising candidate for UV-LED-based white LED applications.

4. Conclusion

In conclusion, the color-changeable new composition Eu^{2+}-doped $Na_{2-x}Al_{2-x}Si_xO_4$ was successfully synthesized using a wet chemical reaction based on TEOS hydrolysis, and its stoichiometry, specifically the x value, could be controlled easily due to the synthesis method. The three different x value-dependent crystal structures were obtained by controlling the ratio of Al or Na to the Si content in that system. Furthermore, the structural distortion of the $Na_{2-x}Al_{2-x}Si_xO_4:Eu^{2+}$ phosphor was strongly dependent on the x value, and the structural distortion induced a transition from a cubic to an orthorhombic phase. Variations in the x value in the $Na_{2-x}Al_{2-x}Si_xO_4:Eu^{2+}$ phosphor caused a change in the PLE and PL spectra, starting with crystal distortion in the host lattice. White LEDs were successfully obtained through the application of $Na_{2-x}Al_{2-x}Si_xO_4:Eu^{2+}$ ($x = 0.25$, 0.35, and 0.55) phosphor to UV-LED chips ($\lambda_{max} = 395$ nm). Preliminary examination found that the three x value-dependent phosphor systems led to improved white LED R_a values. Combination C, in particular, which consisted of blue-emitting $Na_{1.75}Al_{1.75}Si_{0.25}O_4:Eu^{2+}$ and orange-emitting $Na_{1.65}Al_{1.65}Si_{0.35}O_4:Eu^{2+}$, showed a higher R_a value of ~93 and a lower correlated CCT of ~4258 K. Thus, the present phosphor could be a promising candidate as a color-tunable phosphor for white LEDs with high R_a and low CCT values.

Notes and references

1 S. Lee and S. Y. Seo, *J. Electrochem. Soc.*, 2002, **149**, J85.
2 W. B. Im, N. N. Fellows, S. P. DenBaars, R. Seshadri and Y.-I. Kim, *Chem. Mater.*, 2009, **21**, 2957.
3 D. Haranath, H. Chander, P. Sharma and S. Singh, *Appl. Phys. Lett.*, 2006, **89**, 173118.
4 R. Kasuya, A. Kawano, T. Isobe, H. Kuma and J. Katano, *Appl. Phys. Lett.*, 2007, **91**, 111916.
5 Y. Chen, M. Gong, G. Wang and Q. Su, *Appl. Phys. Lett.*, 2007, **91**, 071117.
6 H. S. Jang, W. B. Im, D. C. Lee, D. Y. Jeon and S. S. Kim, *J. Lumin.*, 2007, **126**, 371.
7 K. H. Kwon, W. B. Im, H. S. Jang, H. S. Yoo and D. Y. Jeon, *Inorg. Chem.*, 2009, **48**, 11525.
8 W. B. Im, S. Brinkley, J. Hu, A. Mikhailovsky, S. P. DenBaars and R. Seshadri, *Chem. Mater.*, 2010, **22**, 2842.
9 Y. Wen, Y. Wang, F. Zhang and B. Liu, *Mater. Chem. Phys.*, 2011, **129**, 1171.
10 C.-H. Huang, Y.-C. Chen, T.-M. Chen, T.-S. Chan and H.-S. Sheu, *J. Mater. Chem.*, 2011, **21**, 5645.
11 J. G. Thompson, R. L. Withers, A. Melnitchenko and S. R. Palethorpe, *Acta Crystallogr., Sect. B: Struct. Sci.*, 1998, **54**, 531.
12 R. L. Withers, J. G. Thompson, A. Melnitchenko and S. R. Palethorpe, *Acta Crystallogr., Sect. B: Struct. Sci.*, 1998, **54**, 547.
13 G. Denis, P. Deniard, E. Gautron, F. Clabau, A. Garcia and S. Jobic, *Inorg. Chem.*, 2008, **47**, 4226.
14 M. Zhang, J. Wang, Q. Zhang, W. Ding and Q. Su, *Mater. Res. Bull.*, 2007, **42**, 33.
15 W. Pan, G.-L. Ning, J.-H. Wang and Y. Lin, *Chin. J. Chem.*, 2007, **25**, 605.
16 A. C. Larson and R. B. V. Dreele, *Los Alamos National Laboratory Report LAUR*, 1994.
17 J. G. Thompson, A. Melnitchenko, S. R. Palethorpe and R. L. Withers, *J. Solid State Chem.*, 1997, **131**, 24.
18 Y. Guo, X. Yu, J. Liu and X. Yang, *J. Rare Earths*, 2010, **28**, 34.
19 G. Blasse, W. L. Wanmaker, J. W. Tervrugt and A. Bril, *Philips Res. Rep.*, 1968, **23**, 189.
20 J. K. Park, M. A. Lim, C. H. Kim, H. D. Park and S. Y. Choi, *Electrochem. Solid-State Lett.*, 2004, **7**, H23.
21 H. Zhang, T. Horikawa, H. Hanzawa, A. Hamaguchi and K.-i. Machida, *J. Electrochem. Soc.*, 2007, **154**, J59.
22 P. D. Rack and P. H. Holloway, *Mater. Sci. Eng., R*, 1998, **21**, 171.
23 J. Qiu, K. Miura, N. Sugimoto and K. Hirao, *J. Non-Cryst. Solids*, 1997, **213–214**, 266.
24 R. A. Benhamou, A. Bessière, G. Wallez, B. Viana, M. Elaatmani, M. Daoud and A. Zegzouti, *J. Solid State Chem.*, 2009, **182**, 2319.

25 J. Liu, Y. Wang, X. Yu and J. Li, *J. Lumin.*, 2010, **130**, 2171.
26 W. Y. Shen, M. L. Pang, J. Lin and J. Fangb, *J. Electrochem. Soc.*, 2005, **152**, H25.
27 M. Yu, J. Lin and J. Fang, *Chem. Mater.*, 2005, **17**, 1783.
28 T. Moon, G. Y. Hong, H.-C. Lee, E.-A. Moon, B. W. Jeoung, S.-T. Hwang, J. S. Kim and B.-G. Ryu, *Electrochem. Solid-State Lett.*, 2009, **12**, J61.
29 T. Tsuboi and A. Scacco, *J. Phys.: Condens. Matter*, 1998, **10**, 7259.
30 E. G. Valyashko, S. N. Bodrug, V. N. Mednikova and V. A. Smirnov, *J. Appl. Spectrosc.*, 1977, **26**, 628.
31 J.-C. Krupa and N. A. Kulagin, *Physics of Laser Crystals*, Springer, Netherlands, 2003, vol. 126, pp. 93–107.
32 R. J. Xie, N. Hirosaki, N. Kimura, K. Sakuma and M. Mitomo, *Appl. Phys. Lett.*, 2007, **90**, 191101.